RSC Advances

PAPER

View Article Online
View Journal | View Issue

Cite this: *RSC Adv.*, 2021, **11**, 3012

Understanding the effect of oxide components on proton mobility in phosphate glasses using a statical analysis approach†

Takahisa Omata, *[a] Issei Suzuki, [a] Aman Sharma, [a] Tomohiro Ishiyama, [b] Junji Nishii, [c] Toshiharu Yamashita[d] and Hiroshi Kawazoe[d]

Received 8th December 2020
Accepted 5th January 2021

DOI: 10.1039/d0ra10327f

rsc.li/rsc-advances

The models to describe the proton mobility (μ_H) together with the glass transition temperature (T_g) of proton conducting phosphate glasses employing the glass composition as descriptors have been developed using a statical analysis approach. According to the models, the effects of additional $HO_{1/2}$, MgO, BaO, $LaO_{3/2}$, WO_3, $NbO_{5/2}$, $BO_{3/2}$ and GeO_2 as alternative to $PO_{5/2}$ were found as following. μ_H at T_g is determined first by concentrations of $HO_{1/2}$ and $PO_{5/2}$, and μ_H at T_g increases with increasing $HO_{1/2}$ concentration and decreasing $PO_{5/2}$. The component oxides are categorized into three groups according to the effects on μ_H at T_g and T_g. The group 1 oxides increase μ_H at T_g and decrease T_g, and $HO_{1/2}$, MgO, BaO and $LaO_{3/2}$ and $BO_{3/2}$ are involved in this group. The group 2 oxides increase both μ_H at T_g and T_g, and WO_3 and GeO_2 are involved in this group. The group 3 oxides increase T_g but do not vary μ_H at T_g. Only $NbO_{5/2}$ falls into the group 3 among the oxides examined in this study. The origin of the effect of respective oxide groups on μ_H at T_g and T_g were discussed.

Introduction

Inorganic glasses have been studied for decades as solid electrolytes because of their electrochemical stability and chemical durability, and various cationic conduction, such as Li^+, Ag^+ and H^+ conduction, in oxide glass has been investigated extensively.[1–3] Recent demands for highly proton conducting electrolytes in the temperature range between 250 and 500 °C that is operating temperatures of intermediate temperature fuel cells accelerate to explore proton conducting glasses.[4–9] Our group developed a technique termed as alkali-proton substitution (APS) that injects high concentration of proton carriers, $>10^{21}$ cm^{-3}, into phosphate glasses[10] and fabricated many proton conducting glasses by using APS.[11–14] We studied characteristics of glasses that influence on proton conductivity, such as polymerization level of phosphate framework (ratio of the number of oxygen to phosphorous atoms; O/P ratio)[15] and kinds of glass network modifier,[16] and the effect of additional glass-network formers, such as GeO_2, on the thermal stability.[17] As a result, 2×10^{-3} S cm^{-1} of proton conductivity at 300 °C has been achieved by $34HO_{1/2}$–$2NaO_{1/2}$–$4NbO_{5/2}$–$2BaO$–$4LaO_{3/2}$–$4GeO_2$–$1BO_{3/2}$–$49PO_{5/2}$ glass (36H-glass) up to now.[18] Based on the electromotive force and electrochemical hydrogen pump experiments, the phosphate glass electrolyte is confirmed that the mean transport number of proton is unity even under the oxidation atmosphere like an air electrode atmosphere in the fuel cell,[19] suggesting that highly efficient operation of fuel cells and steam electrolysis cells is achievable owing to its no electronic leakage.[20] In addition, fabrication of ultra-thin glass electrolytes with a thickness of 16 μm was recently demonstrated by the press forming.[21] This will be a great advantage of the glass electrolyte in order to reduce electrolyte resistance (ohmic resistance) of the electrochemical cells. However, further increase of their proton conductivity $>1 \times 10^{-2}$ S cm^{-1} at the operating temperature is still required for practical applications.

Very recently, we have found that the mobility of proton carriers (μ_H) at the glass transition temperature (T_g) in phosphate glasses converges in a small range between 2×10^{-9} and 2×10^{-7} cm^2 V^{-1} s^{-1}, whereas T_g of the glasses is in the wide range of 150 to 650 °C, proton conductivity at 200 °C is also wide range of 10^{-10} to 10^{-4} S cm^{-1}, and proton carrier concentration is in the range of 10^{19} to 10^{22} cm^{-3}.[22] Because the μ_H at T_g of the 36H-glass is 5.4×10^{-8} cm^2 V^{-1} s^{-1} that is the middle in the μ_H at T_g range from 2×10^{-9} to 2×10^{-7} cm^2 V^{-1} s^{-1}, it is suggested that its proton conductivity can be further increased by

[a]*Institute of Multidisciplinary Research for Advanced Materials, Tohoku University, Katahira 2-1-1, Sendai 980-8577, Japan. E-mail: takahisa.omata.c2@tohoku.ac.jp; Fax: +81-22-217-5832; Tel: +81-22-217-5832*

[b]*Fuel Cell Materials Group, Research Institute for Energy Conservation, National Institute of Advanced Industrial Science and Technology (AIST), AIST Central 5, Higashi 1-1-1, Tsukuba, Ibaraki 305-8565, Japan*

[c]*Research Institute for Electronic Science, Hokkaido University, Kita 21 Nishi 10, Kita-ku, Sapporo 001-0021, Japan*

[d]*Kawazoe Frontier Technologies Corporation, Kuden-cho 931-113, Sakae-ku, Yokohama 247-0014, Japan*

† Electronic supplementary information (ESI) available. See DOI: 10.1039/d0ra10327f

improving the μ_H at T_g. Because the determining factor of μ_H at T_g of proton conducting phosphate glasses has yet to be cleared, we unfortunately still do not understand how to improve μ_H at T_g.

The composition of glasses is continuatively controllable unlike the crystalline materials; therefore, various properties of glasses, have been empirically expressed by the mole fraction weighting mean of the respective components.[23–26] Whereas to understand the effects of fundamental properties of glasses, such as O–H bonding, local structure surrounding protons and short range atomic structure of the glass framework, on μ_H at T_g are of course important to understand the proton conduction in phosphate glasses from the physical aspect, understanding the relationship between the glass composition and μ_H at T_g is also valuable in order to improve the electrolyte performance of proton conducting phosphate glasses. When the proton conductivity is successfully described by the glass composition, the proton conductivity of phosphate glasses will be easy to improve based on the obtained relationship between the glass composition and μ_H at T_g, and that will have a major impact on the electrochemical cells such as fuel cells and steam electrolysis cells working at intermediate temperatures. The proton conducting phosphate glasses prepared by using APS previously reported consists of many oxide components;[22] for example, 36H-glass involves 8 oxides as $HO_{1/2}$, $NaO_{1/2}$, BaO, $LaO_{3/2}$, $NbO_{5/2}$, GeO_2, $BO_{3/2}$ and $PO_{5/2}$; therefore, it is not easy to understand the role of the respective component oxides on μ_H at T_g and the relationship between the composition and μ_H at T_g.

Here, we have developed a model, using a statical analysis approach, to describe μ_H at T_g of phosphate glasses according to the glass composition, *i.e.*, the mol% of respective component oxides were employed as descriptors. We also developed a model to describe T_g because the thermal stability of proton conducting glasses is another key property taking the working temperature of the electrochemical devices involving the glasses into account. The effect of respective component oxides on μ_H at T_g and T_g were discussed based on the model obtained.

Methodology

Dataset details

The dataset for μ_H at T_g and T_g of proton conducting phosphate glasses used as training data in this study is referenced from previous report (Table 1 in ref. 16). The dataset has originally 32 records, but for the 13 records in the original dataset, the proton carrier concentrations are smaller than 1 mol% because the proton carrier in those 13 glasses are originated from the residual water. Therefore, we used a dataset that consists of remaining 19 records as summarized in Table 1. Each record contains glass composition in mol% and experimentally determined μ_H at T_g and T_g.

Regression models and method

A linear combination model, in which mol% of respective oxides are used as predictors, is employed for both $\log(\mu_H$ at $T_g)$ and T_g in this study. The regression algorithm used in this study is based on the linear regression as implemented in MATLAB (MathWorks, USA). When the general linear regression was preliminary performed for $\log(\mu_H$ at $T_g)$, the overtraining occurred maybe because of small number of training data; the predicted μ_H at T_g for the 55 296 glass compositions described later was unreasonable values in the range of 10^{-29} to 10^{17} $cm^2\ V^{-1}\ s^{-1}$ (Fig. S1 and S2 in ESI†), although the range of the experimentally observed values is in the range of 2×10^{-9} to 2×10^{-7} $cm^2\ V^{-1}\ s^{-1}$.[22] Therefore, we employed the principal components analysis to fit a linear regression in order to avoid overtraining. Five principal components were employed to explain 95% of variance of original data. The mathematical model can be written as

$$\log\left(\mu_H \text{ at } T_g/\mathrm{cm}^2\ \mathrm{V}^{-1}\ \mathrm{s}^{-1}\right) = a_0 + \sum_{n=1}^{5} a_n \mathrm{PC}_n \quad (1)$$

$$T_g/^\circ\mathrm{C} = b_0 + \sum_{n=1}^{5} b_n \mathrm{PC}'_n \quad (2)$$

$$\mathrm{PC}_n = \sum_i c_i x_i \quad (3)$$

where PC_n and PC'_n are nth principal component explaining the variance of experimentally observed $\log(\mu_H$ at $T_g)$ and T_g, respectively, a_0 and b_0 are intercepts, a_n and b_n are coefficients of nth principal component, x_i is the mol% of the oxide i, and c_i is its coefficient.

In order to check the validity of the models and to understand the effect of respective component oxides on μ_H at T_g and T_g, we performed to predict μ_H at T_g and T_g for 55 296 glass compositions containing 30, 33 and 36 mol% of $HO_{1/2}$, 0, 2 and 4 mol% of WO_3, 0, 2, 4 and 6 mol% of $NbO_{5/2}$, 0, 2, 4 and 6 mol% of MgO, 0, 2, 4 and 6 mol% of BaO, 0, 2, 4 and 6 mol% of $LaO_{3/2}$, 0, 1, 2, 3, 4 and 5 mol% of GeO_2, 0, 1, 2 and 3 mol% of $BO_{3/2}$ and 28–70 mol% of $PO_{5/2}$. In this prediction, all the compositions were assumed to form homogeneous glasses.

Results and discussion

Linear regression models for μ_H at T_g and T_g

The following relationships of $\log(\mu_H$ at $T_g)$ and T_g against the five principal components of glass composition were obtained after regression:

$$\log(\mu_H \text{ at } T_g) = -7.8549 + 0.022233 \times \mathrm{PC}_1 - 0.01167 \times \mathrm{PC}_2 + 0.26874 \times \mathrm{PC}_3 - 0.01727 \times \mathrm{PC}_4 + 0.160456 \times \mathrm{PC}_5, \quad (4)$$

$$T_g = 204.368 - 1.622 \times \mathrm{PC}'_1 + 1.282 \times \mathrm{PC}'_2 - 2.350 \times \mathrm{PC}'_3 + 7.897 \times \mathrm{PC}'_4 + 5.630 \times \mathrm{PC}'_5, \quad (5)$$

The principal components are summarized in Tables 2 and 3 for $\log(\mu_H$ at $T_g)$ and T_g, respectively. Fig. 1(a) and (b) show comparison of experimentally observed and predicted values of μ_H at T_g and T_g, respectively, for the 19 training data. The root mean square error (RMSE) was 0.2775 for $\log(\mu_H$ at $T_g)$ and was

Table 1 Training dataset of the relationship between the glass compositions and the proton mobility (μ_H) at the glass transition temperature (T_g) and T_g

	Mol% of component oxide															
No.	$HO_{1/2}$	$NaO_{1/2}$	WO_3	$NbO_{5/2}$	$TaO_{5/2}$	MgO	BaO	$LaO_{3/2}$	$AlO_{3/2}$	$YO_{3/2}$	$GdO_{3/2}$	GeO_2	$BO_{3/2}$	$PO_{5/2}$	μ_H at T_g ($cm^2\ V^{-1}\ s^{-1}$)	T_g (°C)
1	25	3	1	8	0	0	0	5	0	0	0	0	0	58	2.1×10^{-9}	200
2	24	8	1	8	0	0	0	5	0	0	0	0	0	54	5.5×10^{-9}	177
3	25	10	1	8	0	0	0	5	0	0	0	0	0	51	3.7×10^{-8}	190
4	32	6	1	8	0	0	0	5	0	0	0	0	0	48	3.7×10^{-8}	170
5	32	8	1	8	0	0	0	5	0	0	0	0	0	46	1.2×10^{-8}	167
6	28	2	1	8	0	0	0	5	3	3	0	0	0	50	2.0×10^{-8}	281
7	29	6	1	8	0	0	0	5	3	0	0	0	0	48	7.6×10^{-9}	224
8	30	5	1	8	0	0	0	5	0	3	0	0	0	48	4.1×10^{-9}	228
9	35	0	0	3	0	5	0	3	0	0	0	2	2	50	1.3×10^{-8}	192
10	32	3	0	3	0	0	5	3	0	0	0	2	2	50	6.8×10^{-9}	163
11	34	2	0	4	0	0	2	4	0	0	0	4	1	49	5.4×10^{-8}	180
12	38	2	0	0	4	2	0	4	0	0	0	2	1	47	2.7×10^{-8}	165
13	17	8	0	0	0	0	0	8	0	0	0	1	0	66	2.6×10^{-9}	227
14	12	13	0	0	0	0	0	6	0	0	0	6	0	63	1.3×10^{-8}	243
15	33	2	0	0	0	2	0	5	0	0	0	5	0	53	4.0×10^{-8}	182
16	31	4	0	0	0	2	0	0	0	0	5	5	0	53	1.2×10^{-8}	178
17	20	5	0	0	0	0	0	6	0	0	0	6	0	63	1.5×10^{-8}	252
18	28	7	0	0	0	2	0	0	0	0	5	5	0	53	1.4×10^{-8}	233
19	34	1	8	8	0	0	0	5	0	0	0	0	0	44	1.1×10^{-7}	231

Table 2 Five principal components obtained from the analysis of μ_H at T_g

Principal components		PC_1	PC_2	PC_3	PC_4	PC_5
Proportion of variance		0.659	0.183	0.061	0.026	0.021
Cumulative proportion		0.659	0.842	0.903	0.929	0.950
Factor loading	$x(HO_{1/2})$	0.69239	−0.32693	−0.07750	−0.19571	−0.15439
	$x(NaO_{1/2})$	−0.24549	0.28854	0.71623	−0.35865	−0.03489
	$x(WO_3)$	0.06837	0.15986	−0.11444	0.32222	0.77387
	$x(NbO_{5/2})$	0.16670	0.68417	−0.16598	0.28247	−0.30664
	$x(TaO_{5/2})$	0.02694	−0.05991	0.00355	−0.24336	0.04874
	$x(MgO)$	0.03954	−0.18457	0.01768	0.06160	−0.13778
	$x(BaO)$	0.02319	−0.04547	−0.02005	−0.12335	−0.09325
	$x(LaO_{3/2})$	−0.08309	0.19943	−0.33952	−0.50726	0.26128
	$x(AlO_{3/2})$	0.01281	0.06277	−0.04134	0.08739	−0.09090
	$x(YO_{3/2})$	0.01467	0.05828	−0.05950	0.09692	−0.09979
	$x(GdO_{3/2})$	−0.00319	−0.15212	0.31784	0.52266	−0.11954
	$x(GeO_2)$	−0.10164	−0.37370	0.21746	0.08717	0.28694
	$x(BO_{3/2})$	0.02654	−0.05917	−0.04343	−0.10435	−0.08555
	$x(PO_{5/2})$	−0.63774	−0.25119	−0.41100	0.07224	−0.24811

23.6 °C for T_g. No systematic error was observed and the fitting were reasonably good for both $\log(\mu_H$ at $T_g)$ and T_g. Fig. 2(a) and (b) respectively show the predicted values of $\log(\mu_H$ at $T_g)$ and T_g for the 55 296 phosphate glass compositions. The predicted values are ranging between 8.1×10^{-10} and 7.7×10^{-7} $cm^2\ V^{-1}\ s^{-1}$ for μ_H at T_g and between 152 and 256 °C for T_g. As compared with experimentally determined μ_H at T_g,[22] the range of the predicted values are very close to the range of the experimentally observed values from 2×10^{-9} to 2×10^{-7} $cm^2\ V^{-1}\ s^{-1}$. These results indicate that the models obtained are quite reasonable and available to discuss the effects of respective component oxides on μ_H at T_g.

As seen in Table 2, absolute values of the factor loading of $HO_{1/2}$ and $PO_{5/2}$ components are particularly larger than those of the other components, indicating that μ_H at T_g is first determined by the concentration of $HO_{1/2}$ and $PO_{5/2}$. Taking into account that the coefficient of PC_1 in eqn (4) is positive, μ_H at T_g increases with the increasing $HO_{1/2}$ concentration, and it reduces with the increasing $PO_{5/2}$ concentration. In this respect, the experimental observation that the μ_H increases with the decreasing polymerization level of phosphate glass-network is reproduced well by the present model. μ_H turns into decrease at O/P ratio (ratio of the number of oxygen to phosphorous atoms) higher than 3.5–3.6;[15] however, such a behavior cannot be reproduced using linear regression model. Consequently, applicable composition range of the present model is limited in a O/P ratio smaller than 3.5–3.6.

Table 3 Five principal components obtained from the analysis of T_g

Principal components		PC'_1	PC'_2	PC'_3	PC'_4	PC'_5
Proportion of variance		0.659	0.183	0.061	0.026	0.021
Cumulative proportion		0.659	0.842	0.903	0.929	0.950
Factor loading	$x(HO_{1/2})$	0.69239	−0.32693	−0.0775	−0.19571	−0.15439
	$x(NaO_{1/2})$	−0.24549	0.28854	0.71623	−0.35865	−0.03489
	$x(WO_3)$	0.06837	0.15986	−0.11444	0.32222	0.77387
	$x(NbO_{5/2})$	0.1667	0.68417	−0.16598	0.28247	−0.30664
	$x(TaO_{5/2})$	0.02694	−0.05991	0.00355	−0.24336	0.04874
	$x(MgO)$	0.03954	−0.18457	0.01768	0.0616	−0.13778
	$x(BaO)$	0.02319	−0.04547	−0.02005	−0.12335	−0.09325
	$x(LaO_{3/2})$	−0.08309	0.19943	−0.33952	−0.50726	0.26128
	$x(AlO_{3/2})$	0.01281	0.06277	−0.04134	0.08739	−0.0909
	$x(YO_{3/2})$	0.01467	0.05828	−0.0595	0.09692	−0.09979
	$x(GdO_{3/2})$	−0.00319	−0.15212	0.31784	0.52266	−0.11954
	$x(GeO_2)$	−0.10164	−0.3737	0.21746	0.08717	0.28694
	$x(BO_{3/2})$	0.02654	−0.05917	−0.04343	−0.10435	−0.08555
	$x(PO_{5/2})$	−0.63774	−0.25119	−0.411	0.07224	−0.24811

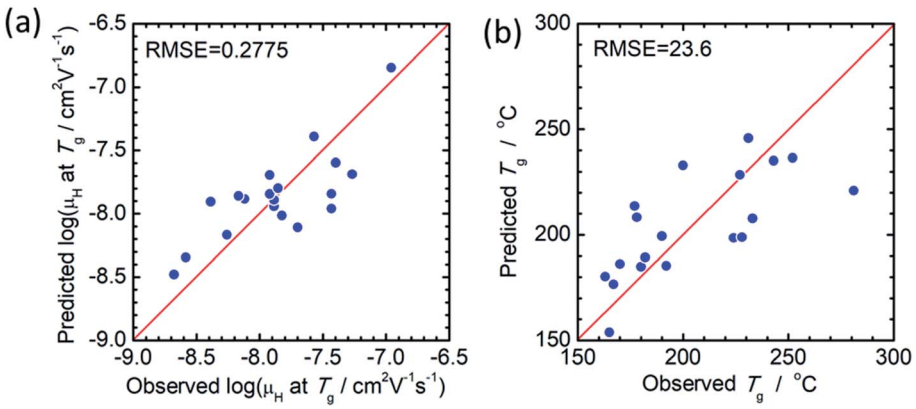

Fig. 1 Comparison of experimentally observed and predicted values of (a) μ_H at T_g and (b) T_g.

From comparison of the models of μ_H at T_g and T_g as summarized in Tables 2 and 3, the factor loadings of respective principal components for log(μ_H at T_g) and T_g are surprisingly found to be the same each other, *i.e.*, the variance in both log(μ_H at T_g) and T_g are explained by the same principal components, clearly indicating that there should be some kind of relationship between log(μ_H at T_g) and T_g. This is quite consistent with our previously reported estimation that the motion of protons (proton diffusion or mobility) determines the motion of glass framework (T_g) in the proton conducting phosphate glasses.[22] Fig. 3 shows log(μ_H at T_g) as a function of T_g of 55 296 predicted values (black dots) together with the experimentally observed 19 values (red dots). A trend that log(μ_H at T_g) decreases linearly with the increasing T_g was clearly observed for the predicted

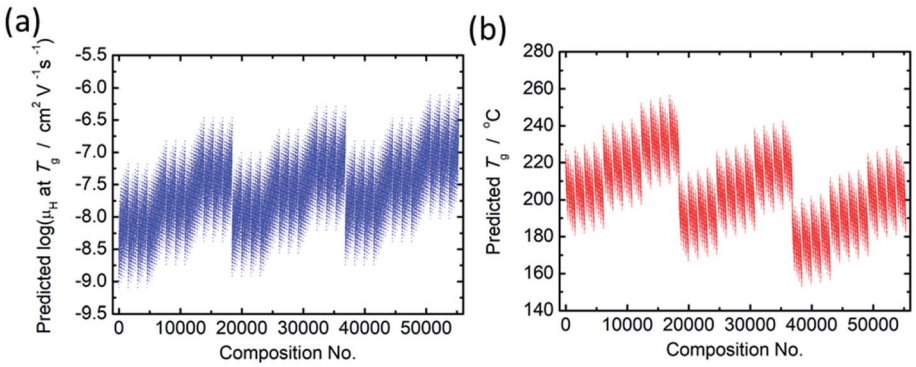

Fig. 2 Predicted values of (a) log(μ_H at T_g) and (b) T_g for the 55 296 phosphate glass compositions.

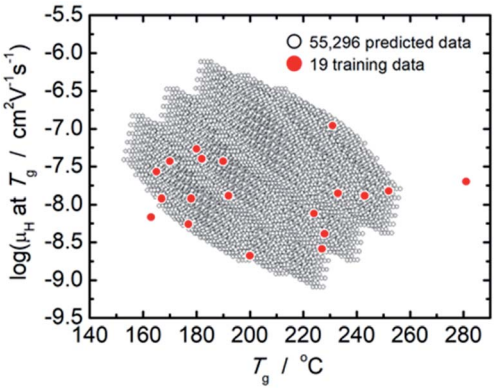

Fig. 3 Plot of $\log(\mu_H$ at $T_g)$ as a function of T_g of 55 296 predicted values (open black dots) together with the experimentally observed 19 values (closed red dots).

values in Fig. 3. The observed relationship between $\log(\mu_H$ at $T_g)$ and T_g may be a key to understand physical factor to determine μ_H at T_g; however, we need additional information in order to go further this problem. Therefore, the origin of the relationship between $\log(\mu_H$ at $T_g)$ and T_g remains as an open question, and we do not discuss further in this paper.

Effects of respective component oxides on μ_H at T_g and T_g

As mentioned in the previous section, there is a clear relationship between $\log(\mu_H$ at $T_g)$ and T_g; therefore, the effect of each component oxide was studied in this regard. Fig. 4 shows the distribution of relationship between $\log(\mu_H$ at $T_g)$ and T_g depending on the concentration of respective component oxides. All data plotted in Fig. 4 are predicted values. In Fig. 4(a), 55 296 predicted values are distinguished into three parts depending on the concentration of $HO_{1/2}$. In Fig. 4(b), 18 432 predicted values for the glasses with 30 mol% of $HO_{1/2}$ are plotted and they are distinguished into three parts depending on the concentration of WO_3. In Fig. 4(c), 6144 predicted values for the glasses with 30 mol% of $HO_{1/2}$ and 0 mol% of WO_3 are plotted and they are distinguished into four parts depending on the concentration of $LaO_{3/2}$. In Fig. 4(d), (e), (f), (g) and (h), 1536 predicted values for the glasses with 30 mol% of $HO_{1/2}$, 0 mol% of WO_3 and 0 mol% of $LaO_{3/2}$ are plotted and they are distinguished into four or six parts depending on the concentration of the oxide of interest (MgO, BaO, $NbO_{5/2}$, $BO_{3/2}$ and GeO_2). The situation observed, when the component oxide of interest adds into the glass as alternative to $PO_{5/2}$, is described as follows.

With the increasing $HO_{1/2}$ concentration (Fig. 4(a)), the T_g decreases by 5 °C per 1 mol% $HO_{1/2}$ and $\log(\mu_H$ at $T_g)$ increases by 0.06 per 1 mol% of $HO_{1/2}$. In contrast to the dependence of $HO_{1/2}$ concentration, both T_g and $\log(\mu_H$ at $T_g)$ increases with the increasing WO_3 concentration by 6.5 °C and 0.08 per 1 mol% of WO_3, respectively (Fig. 4(b)). In the case of $LaO_{3/2}$ shown in Fig. 4(c), T_g decreases with the increasing $LaO_{3/2}$ concentration by 2.2 °C per 1 mol% of $LaO_{3/2}$, and $\log(\mu_H$ at $T_g)$ increases with the increasing $LaO_{3/2}$ concentration by 0.1 per 1 mol% of $LaO_{3/2}$. In the cases for MgO, BaO and $BO_{3/2}$ shown in Fig. 4(d), (e) and (f), respectively, the dependence are similar to the case of $HO_{1/2}$ and $LaO_{3/2}$; T_g decreases and $\log(\mu_H$ at $T_g)$ increases with the increasing concentration of the additional oxide. The variation in T_g and $\log(\mu_H$ at $T_g)$ are respectively −1.5 °C and 0.05 per 1 mol% of MgO, −2.4 °C and 0.05 per 1 mol% of BaO and −2.2 °C and 0.05 per 1 mol% of $BO_{3/2}$. For $NbO_{5/2}$, as clearly seen in Fig. 4(g), the relationship between $\log(\mu_H$ at $T_g)$ and T_g is little dependent on the $NbO_{5/2}$ concentration, *i.e.*, T_g increases by 0.7 °C per 1 mol% of $NbO_{5/2}$ and $\log(\mu_H$ at $T_g)$ does not change regardless $NbO_{5/2}$ concentration. In the case of GeO_2 shown in Fig. 4(h), both T_g and $\log(\mu_H$ at $T_g)$ increases with the increasing GeO_2 concentration similar to the case of WO_3; however, increase in T_g, 0.6 °C per 1 mol% of GeO_2, is much smaller than that of WO_3 (6.5 °C per 1 mol% of WO_3), while increase in $\log(\mu_H$ at $T_g)$, 0.12 per 1 mol% of GeO_2, is slightly larger than that of WO_3 (0.08 per 1 mol% of WO_3). These situations are summarized in Table 4.

It is noticed that the component oxides are categorized into three groups in terms of the effect on the μ_H at T_g and T_g. The group 1 consists of $HO_{1/2}$, MgO, BaO, $LaO_{3/2}$ and $BO_{3/2}$. They increase μ_H at T_g but decrease T_g, when their concentrations increase. The group 2 involves WO_3 and GeO_2 that increase both μ_H at T_g and T_g, when their concentrations increase. The group 3 consists of $NbO_{5/2}$ only in the present study, and it increases T_g but does not changes μ_H at T_g, when its concentration increases. Such effects categorized into three groups could not be found in the experimentally observed data, *i.e.*, 19 glass compositions that used as training data in this study. The information of the three groups is useful to obtain purpose-designed glasses.

The effect on T_g of respective group oxides is quite reasonable and explained according to the glass structural chemistry as following. The group 1 consists of the glass-modifiers except for $BO_{3/2}$; therefore, the reduction of T_g with the increasing concentration of the group 1 oxide is reasonably understood as a result of breaking of the phosphate glass-network by introduction of the glass-modifier oxides. $BO_{3/2}$ is a glass-former oxide, and it may exist in the glass as the trigonal planer BO_3 in addition to the BO_4 tetrahedron in the phosphate glasses assumed in the present study.[27–29] When the trigonal planer BO_3 is introduced into the glass as alternative to PO_4 tetrahedra, the number of the bridging oxygens in the glass-network reduces as the concentration of the trigonal planer BO_3 increases. Consequently, $BO_{3/2}$ acts as almost glass-modifier, and its effect on T_g is similar to the other group 1 oxides that are glass-modifier oxides. The groups 2 and 3 consist of the oxides exhibiting high glass forming ability, *i.e.*, GeO_2 is a glass-former and WO_3 and $NbO_{5/2}$ are conditional glass-formers.[30] When the groups 2 and 3 oxides are introduced into the glass as alternative to $PO_{5/2}$, GeO_2 tetrahedra and WO_6 and NbO_6 octahedra strengthen the phosphate glass-network, resulting in increasing T_g.

In contrast to the effect on T_g, the origin of the effect on μ_H at T_g is still an open question as already mentioned. However, the effect of the group 2 oxides, *i.e.*, they increase μ_H at T_g with the increasing their concentration, may be explained phenomenologically as following. For the effect of WO_3, we refer to the heteropoly acid of WO_3 combined with $PO_{5/2}$. It is well known

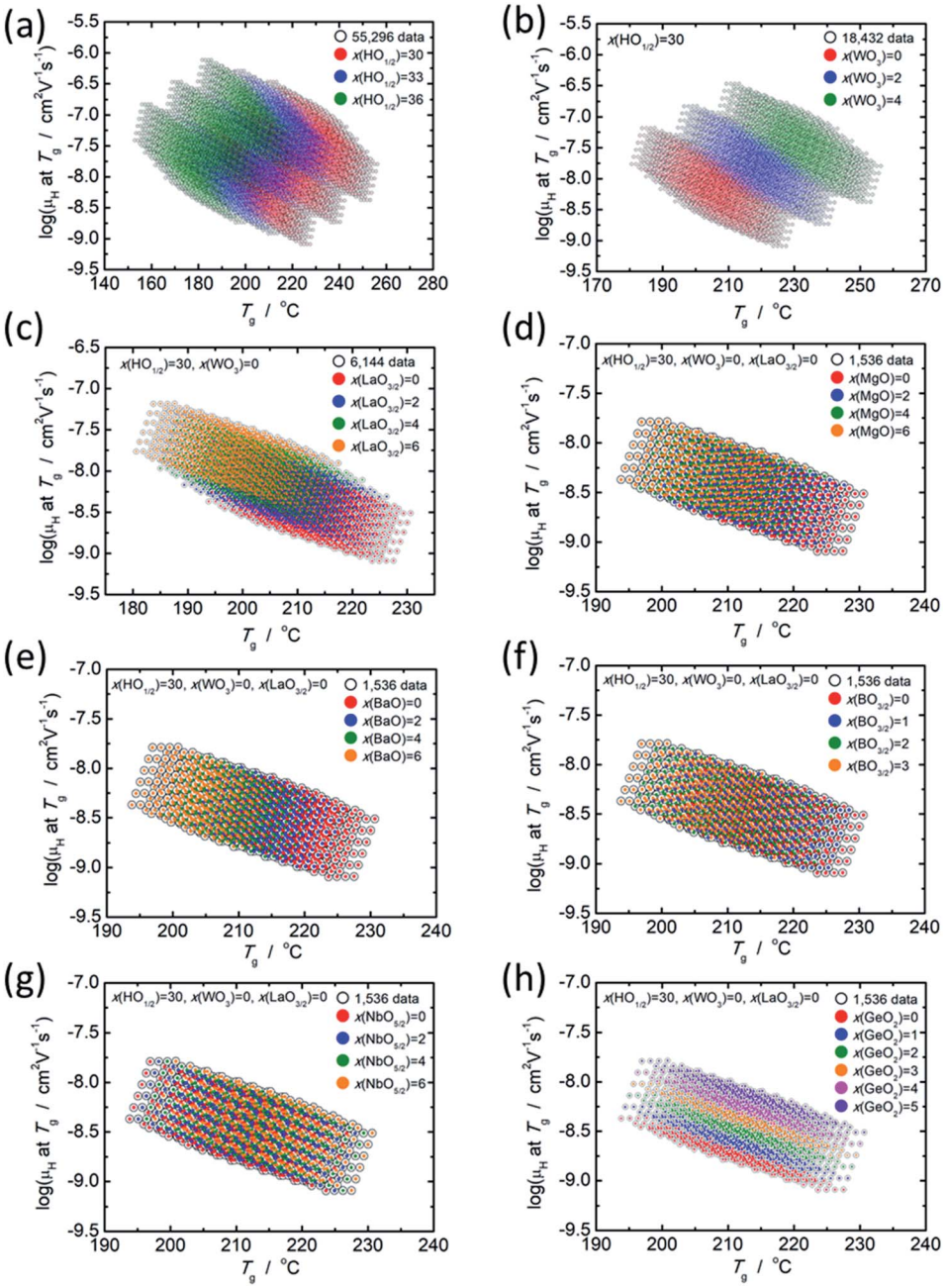

Fig. 4 Distribution of the relationship between predicted values of $\log(\mu_H$ at $T_g)$ and T_g depending on the concentration of respective component oxides. (a) 55 296 predicted values distinguished by the $HO_{1/2}$ concentration (red dots = 30 mol% $HO_{1/2}$, blue dots = 33 mol% $HO_{1/2}$ and green dots = 36 mol% $HO_{1/2}$), (b) 18 432 predicted values for the glasses with 30 mol% of $HO_{1/2}$ distinguished by the WO_3 concentration (red dots = 0 mol% WO_3, blue dots = 2 mol% WO_3 and green dots = 4 mol% WO_3), (c) 6144 predicted values for the glasses with 30 mol% of $HO_{1/2}$ and 0 mol% of WO_3 distinguished by the $LaO_{3/2}$ concentration (red dots = 0 mol% $LaO_{3/2}$, blue dots = 2 mol% $LaO_{3/2}$, green dots = 4 mol% $LaO_{3/2}$ and orange dots = 6 mol% $LaO_{3/2}$). (d), (e), (f), (g) and (h) 1536 predicted values for the glasses with 30 mol% of $HO_{1/2}$, 0 mol% of WO_3 and 0 mol% of $LaO_{3/2}$ respectively distinguished by the concentration of MgO, BaO, $BO_{3/2}$, $NbO_{5/2}$ and GeO_2.

Table 4 Variation of $\log(\mu_H$ at $T_g)$ and T_g with the increasing component oxide by 1 mol%

		Group 1				Group 2		Group 3
Component oxide		MgO	BaO	$LaO_{3/2}$	$BO_{3/2}$	WO_3	GeO_2	$NbO_{5/2}$
Variation per 1 mol% of oxide	$\log(\mu_H$ at $T_g)$	0.05	0.05	0.10	0.05	0.08	0.12	0.00
	T_g/°C	−1.5	−2.4	−2.2	−2.2	6.5	0.6	0.7

that WO_3 and $PO_{5/2}$ form heteropoly acid, $H_3PW_{12}O_{40}\cdot 6H_2O$, and it exhibits strong acidity much stronger than H_2SO_4.[31,32] The strong acidity, *i.e.*, easy proton formation, is explained by dispersion of the negative charge over many atoms of the polyanion, $PW_{12}O_{40}^{3-}$, and the polarization of the outer W=O bond.[32] Of course, the molar ratio of WO_3 over against $PO_{5/2}$ is much smaller (4 mol% of WO_3 is the highest, while 28 mol% of $PO_{5/2}$ is the lowest) than that of $PW_{12}O_{40}^{3-}$; therefore, formation of $PW_{12}O_{40}^{3-}$-like polyanion should be excluded. However, the WO_3 coexisting with $PO_{5/2}$ may have an effect to enhance acidity of ≡P–O–H units. In this case, protons are easy to dissociate from ≡P–O–H units; as a result, μ_H would be increased by the addition of WO_3 into phosphate glasses.

In the case of GeO_2, we refer to the silicophosphate gel that is prepared by reacting $SiCl_4$ with anhydrous phosphoric acid (H_3PO_4).[33] The silicophosphate gel that involves Si–O–P bondings exhibits evidently higher proton conductivity than H_3PO_4,[33,34] although the increase in conductivity is not so large. Taking into account that the polymerization occurs in silicophosphate gel, the concentration of proton carriers in silicophosphate is smaller than that in phosphoric acid, indicating that the SiO_2 addition enhances μ_H. Although the reason why SiO_2 addition enhance proton conductivity has not been fully understood yet, the octahedrally coordinated SiO_6 that appears in silicophosphate gel is pointed out as a key feature to explain the effect of SiO_2 addition into phosphoric acid.[33] While GeO_2 exhibits similar feature to SiO_2, *i.e.*, both GeO_2 and SiO_2 are group 4 oxides and exhibit as glass-formers, preference of six-fold coordination of Ge^{4+} ion is higher than Si^{4+} ion. These imply that GeO_2 would enhance μ_H, when it is added into the phosphoric acid. In this case, increase in μ_H by the addition of GeO_2 to phosphate glass would be understood by the analogous to silicophosphate gel.

Conclusion

In summary, we developed a linear regression models for the compositional dependence of $\log(\mu_H \text{ at } T_g)$ and T_g for the proton conducting phosphate glass based on the approach of principal component analysis, and μ_H at T_g and T_g were predicted for 55 296 of phosphate glasses involving 9 component oxide of $HO_{1/2}$, MgO, BaO, $LaO_{3/2}$, WO_3, $NbO_{5/2}$, $BO_{3/2}$, GeO_2 and $PO_{5/2}$. The models themselves do not have any physical meaning of course, but they provide the following information about the effects of respective component oxides on μ_H at T_g and T_g: (i) the μ_H at T_g is determined first by concentrations of $HO_{1/2}$ and $PO_{5/2}$; μ_H at T_g increases with increasing $HO_{1/2}$ concentration and decreasing $PO_{5/2}$. (ii) There is a trend for $\log(\mu_H \text{ at } T_g)$ to increase linearly as T_g decreases. This is quite consistent with our estimation previously reported that the motion of protons determines the motion of glass framework in the proton conducting phosphate glasses. (iii) The component oxides are categorized into three groups according to the effects on μ_H at T_g and T_g. The group 1 oxides that behave as glass-modifiers increase μ_H at T_g and decrease T_g, and $HO_{1/2}$, MgO, BaO and $LaO_{3/2}$ and $BO_{3/2}$ are involved in this group. The group 2 oxides increase both μ_H at T_g and T_g, and WO_3 and GeO_2 are involved in this group. The group 3 oxides increase T_g but do not vary μ_H at T_g. Only $NbO_{5/2}$ falls into the group 3 among the oxides examined in this study. These information are very useful to obtain purpose-designed glasses; therefore, they will be applied to the future development of proton-conducting phosphate glasses. Especially, the effects of the additional glass-formers, such as GeO_2 and WO_3, are very important to design highly proton conducting phosphate glass at intermediate temperatures.

The enhance of μ_H at T_g by WO_3 and GeO_2 of group 2 oxide is phenomenologically understood by referring to the strong acidity of $PW_{12}O_{40}^{3-}$ heteropoly acid and the enhancing μ_H of phosphoric acid by SiO_2 addition, respectively. In contrast, the origin of the effect of groups 1 and 3 oxides on μ_H at T_g and the relationship between $\log(\mu_H \text{ at } T_g)$ and T_g still remain as open questions.

Author contributions

Takahisa Omata: conceptualization, methodology, formal analysis, software, writing – original draft and visualization, Issei Suzuki: validation, visualization and writing – review & editing, Aman Sharma: formal analysis and data curation, Tomohiro Ishiyama: writing – review & editing, Junji Nishii: conceptualization, funding acquisition and writing – review & editing, Toshiharu Yamashita: supervision and writing – review & editing, Hiroshi Kawazoe: supervision and writing – review & editing.

Conflicts of interest

The authors declare no competing interests.

Acknowledgements

We thank Prof. Junichi Kawamura (Tohoku University) for valuable comments. This work was supported in part by a Grant-in-Aid for Scientific Research (B) (Grant No. 20H02428). This work was partly performed under the Cooperative Research Program of the "Network Joint Research Center for Materials and Devices" (No. 20194020 and 20204012) and "Dynamic Alliance for Open Innovation Bridging Human, Environment, and Materials".

References

1 A. Hayashi, A. Sakuda and M. Tatsumisago, *Front. Energy Res.*, 2016, **4**, 1–13.
2 M. Nakayama, M. Hanaya, A. Hatate and M. Oguni, *J. Non-Cryst. Solids*, 1994, **172–174**, 1252–1261.
3 Y. Abe, H. Hosono, O. Akita and L. L. Hench, *J. Electrochem. Soc.*, 1994, **141**, L64–L65.
4 Y. Daiko, *J. Ceram. Soc. Jpn.*, 2013, **121**, 539–543.
5 Y. Takamatsu, Y. Daiko, S. Kohara, K. Suzuya, A. Mineshige and T. Yazawa, *Solid State Ionics*, 2013, **245–246**, 19–23.
6 H. Sumi, Y. Nakano, Y. Fujishiro and T. Kasuga, *Solid State Sci.*, 2015, **45**, 5–8.

7 Y. Huang, E. Christensen, Q. Shuai and Q. Li, *Int. J. Hydrogen Energy*, 2017, **42**, 7235–7240.
8 H. Sumi, *J. Ceram. Soc. Jpn.*, 2017, **125**, 829–832.
9 S. H. Lee, S. B. Park and Y. Il Park, *Solid State Ionics*, 2020, **345**, 115186.
10 T. Ishiyama, S. Suzuki, J. Nishii, T. Yamashita, H. Kawazoe and T. Omata, *J. Electrochem. Soc.*, 2013, **160**, E143–E147.
11 T. Ishiyama, S. Suzuki, J. Nishii, T. Yamashita, H. Kawazoe and T. Omata, *Solid State Ionics*, 2014, **262**, 856–859.
12 T. Ishiyama, J. Nishii, T. Yamashita, H. Kawazoe and T. Omata, *J. Mater. Chem. A*, 2014, **2**, 3940–3947.
13 T. Yamaguchi, T. Ishiyama, K. Sakuragi, J. Nishii, T. Yamashita, H. Kawazoe and T. Omata, *Solid State Ionics*, 2015, **275**, 22855–22861.
14 T. Yamaguchi, T. Ishiyama, K. Sakuragi, J. Nishii, T. Yamashita, H. Kawazoe, N. Kuwata, J. Kawamura and T. Omata, *Solid State Ionics*, 2016, **288**, 281–285.
15 T. Yamaguchi, T. Kataoka, S. Tsukuda, T. Ishiyama, J. Nishii, T. Yamashita, H. Kawazoe and T. Omata, *Phys. Chem. Chem. Phys.*, 2017, **19**, 29669–29675.
16 T. Yamaguchi, Y. Saito, Y. Kuwahara, H. Yamashita, T. Ishiyama, J. Nishii, T. Yamashita, H. Kawazoe and T. Omata, *J. Mater. Chem. A*, 2017, **5**, 12385–12392.
17 K. Kawaguchi, T. Yamaguchi, T. Omata, T. Yamashita, H. Kawazoe and J. Nishii, *Phys. Chem. Chem. Phys.*, 2015, **17**, 22855–22861.
18 T. Yamaguchi, S. Tsukuda, T. Ishiyama, J. Nishii, T. Yamashita, H. Kawazoe and T. Omata, *J. Mater. Chem. A*, 2018, **6**, 23628–23637.
19 T. Ishiyama, H. Kishimoto, K. Yamaji, T. Yamaguchi, J. Nishii, T. Yamashita, H. Kawazoe and T. Omata, *Int. J. Hydrogen Energy*, 2019, **44**, 24977–24984.
20 T. Nakamura, S. Mizunuma, Y. Kimura, Y. Mikami, K. Yamauchi, T. Kuroha, N. Taniguchi, Y. Tsuji, Y. Okuyama and K. Amezawa, *J. Mater. Chem. A*, 2018, **6**, 15771–15780.
21 I. Suzuki, M. Tashiro, T. Yamaguchi, T. Ishiyama, J. Nishii, T. Yamashita, H. Kawazoe and T. Omata, *Int. J. Hydrogen Energy*, 2020, **45**, 16690–16697.
22 T. Omata, T. Yamaguchi, S. Tsukuda, T. Ishiyama, J. Nishii, T. Yamashita and H. Kawazoe, *Phys. Chem. Chem. Phys.*, 2019, **21**, 10744–10749.
23 T. Kentaro, *J. Ceram. Assoc. Jpn.*, 1955, **63**, 142–147.
24 A. Makishima and J. D. Mackenzie, *J. Non-Cryst. Solids*, 1973, **12**, 35–45.
25 B. Deng, *J. Non-Cryst. Solids*, 2020, **529**, 119768.
26 S. Bishnoi, S. Singh, R. Ravinder, M. Bauchy, N. N. Gosvami, H. Kodamana and N. M. A. Krishnan, *J. Non-Cryst. Solids*, 2019, **524**, 119643.
27 N. Mascaraque, A. Durán and F. Muñoz, *J. Non-Cryst. Solids*, 2011, **357**, 3212–3220.
28 S. Le Roux, S. Martin, R. Christensen, Y. Ren and V. Petkov, *J. Phys.: Condens. Matter*, 2011, **23**, 035403.
29 R. K. Brow and D. R. Tallant, *J. Non-Cryst. Solids*, 1997, **222**, 396–406.
30 N. Boubata, A. Roula and I. Moussaoui, *Bull. Mater. Sci.*, 2013, **36**, 457–460.
31 I. V. Kozhevnikov and K. I. Matveev, *Appl. Catal.*, 1983, **5**, 135–150.
32 M. Makoto, *Mater. Chem. Phys.*, 2002, **75**, 103–120.
33 Y. Ansari, T. G. Tucker and C. A. Angell, *J. Power Sources*, 2013, **237**, 47–51.
34 Y. Ansari, T. G. Tucker, W. Huang, I. S. Klein, S. Y. Lee, J. L. Yarger and C. A. Angell, *J. Power Sources*, 2016, **303**, 142–149.